

Avalanche Mechanism for the Enhanced Loss of Ultracold Atoms

Christian Langmack, D. Hudson Smith, and Eric Braaten

Department of Physics, The Ohio State University, Columbus, OH 43210, USA

(Dated: March 5, 2022)

Abstract

In several experiments with ultracold trapped atoms, a narrow loss feature has been observed near an *atom-dimer resonance*, at which there is an Efimov trimer at the atom-dimer threshold. The conventional interpretation of these loss features is that they are produced by the *avalanche mechanism*, in which the energetic atom and dimer from 3-body recombination undergo secondary elastic collisions that produce additional atoms with sufficient energy to escape from the trapping potential. We use Monte Carlo methods to calculate the average number of atoms lost and the average heat generated by recombination events in a Bose-Einstein condensate and in a thermal gas. We improve on previous models by taking into account the energy-dependence of the cross sections, the spacial structure of the atom cloud, and the elastic scattering of the atoms. We show that the avalanche mechanism cannot produce a narrow loss feature near the atom-dimer resonance. The number of atoms lost from a recombination event can be more than twice as large as the 3 that would be obtained in the absence of secondary collisions. However the resulting loss feature is broad and its peak is at a scattering length that is larger than the atom-dimer resonance and depends on the trap depth.

PACS numbers: 31.15.-p,34.50.-s,03.75.Nt

Keywords: Degenerate Bose gases, three-body recombination, scattering of atoms and molecules.

I. INTRODUCTION

Particles with short-range interactions and an S-wave scattering length a that is large compared to the range have universal low-energy properties that depend on a but not on other details of the interactions or on the structure of the particles [1]. This universality provides deep connections between various fields of physics, including atomic and molecular, condensed matter, nuclear, and particle physics. It has stimulated dramatic advances in theoretical and experimental few-body physics – particularly in the study of the universal few-body reaction rates of ultracold atoms.

Since particles with large scattering length are essentially indivisible at low energies, we refer to them as *atoms*. In the 2-atom sector, the universal properties are simple. If $a > 0$, they include the existence of a loosely-bound diatomic molecule that we refer to as the *shallow dimer*. In the 3-atom sector, the universal properties are more intricate. In many cases, including identical bosons, they include the existence of a sequence of universal triatomic molecules called *Efimov trimers* that were discovered by Efimov in 1970 [2]. In the zero-range limit, the spectrum of Efimov trimers is invariant under discrete scale transformations [3]. For identical bosons, the discrete scaling factor is approximately 22.7. Reaction rates among three low-energy atoms also respect discrete scale invariance [4]. We refer to universal few-body phenomena with discrete scaling behavior as *Efimov physics*.

Ultracold trapped atoms provide an ideal laboratory for studying Efimov physics, because the scattering length can be controlled experimentally using Feshbach resonances. The simplest probes of Efimov physics are loss features: local maxima and minima in the atom loss rate as functions of the scattering length a . The most dramatic signature of an Efimov trimer is the resonant enhancement of the 3-body recombination rate near a negative value of a for which there is an Efimov trimer at the 3-atom threshold [5]. The first observation of such a loss feature in an ultracold gas of ^{133}Cs atoms [6] revealed a line shape consistent with universal predictions [7].

In a mixture of atoms and shallow dimers, a narrow loss feature can also be caused by an Efimov trimer near the atom-dimer threshold. We refer to a scattering length a_* for which an Efimov trimer is exactly at the threshold as an *atom-dimer resonance*. For a near a_* , there is resonant enhancement near threshold of the elastic scattering of an atom and the shallow dimer. There is also resonant enhancement of their inelastic scattering into an atom and a more tightly-bound diatomic molecule, which we refer to as a *deep dimer*. The release of the large binding energy of the deep dimer gives the outgoing atom and dimer large enough kinetic energies to escape from the trapping potential. The resulting peaks in the atom and dimer loss rates near a_* were first observed in a mixture of ^{133}Cs atoms and dimers [8].

There have also been observations of narrow loss features near an atom-dimer resonance in systems consisting of atoms only. Zaccanti et al. observed a narrow loss peak near the predicted position of a_* in a Bose-Einstein condensate of ^{39}K atoms [9]. They also observed a loss peak in a thermal gas near the next atom-dimer resonance, at a scattering length larger by a factor of about 22.7. Pollack et al. observed a loss peak near the predicted position of an atom-dimer resonance in a Bose-Einstein condensate of ^7Li atoms [10]. Machtay et al. observed such a loss peak in a thermal gas of ^7Li atoms [11]. These loss features near the atom-dimer resonance are puzzling, because the equilibrium population of shallow dimers is expected to be negligible in these systems. Thus, any losses due to inelastic scattering between an atom and a shallow dimer should be negligible.

Zaccanti et al. proposed an *avalanche mechanism* for the enhancement of the atom loss rate near an atom-dimer resonance in systems consisting of atoms only [9]. Near a_* , atom-dimer cross sections are resonantly enhanced near threshold. Each 3-body recombination event produces an atom and a shallow dimer with kinetic energies much larger than that required to escape from the trap. If the atom and dimer both escape, 3 atoms are lost. If the dimer instead scatters inelastically, the scattered atom is also lost, so the number of atoms lost is 4. However the dimer can undergo one or more elastic collisions before ultimately escaping or suffering an inelastic collision, and the scattered atoms may gain enough energy to escape from the trap. The scattered atoms may also undergo elastic collisions, producing still more lost atoms. Thus the dimer could initiate an avalanche of lost atoms. The atom from the recombination event could also initiate an avalanche of lost atoms. Thus the number of atoms lost could be significantly larger than 3. Near a_* , the resonant enhancement of the atom-dimer elastic cross section increases the probability for the dimer to undergo an elastic collision and initiate an avalanche. This suggests that there should be an increase in the number of atoms lost per recombination event near a_* . If the increase is sufficiently narrow, it could be observed as a local maximum in the atom loss rate. Zaccanti et al. proposed this avalanche mechanism as an explanation for the loss features near the atom-dimer resonance. They also developed a model for calculating the number of atoms lost that demonstrated the plausibility of the avalanche mechanism [9].

In Ref. [12], we analyzed the avalanche mechanism for atom loss and concluded that it was unable to produce a narrow loss feature near an atom-dimer resonance. In this paper, we present a more thorough analysis of the avalanche mechanism. We use Monte Carlo methods to generate avalanches of atoms that are initiated by recombination events and then calculate the number of atoms lost by averaging over avalanches. We confirm that this number can be significantly larger than the naive value 3. However, instead of a narrow peak in the atom loss rate near a_* , the avalanche mechanism produces a broad enhancement whose maximum is at a larger value of a .

This paper is organized as follows. In Section II, we summarize the few-body physics that is used in our Monte Carlo model for the avalanche mechanism. In Section III, we describe the experimental inputs that are required in the Monte Carlo model. In Section IV, we present the Monte Carlo method for generating avalanches initiated by 3-body recombination events. In Section V, we apply the Monte Carlo model to experiments on ^7Li , ^{39}K , and ^{133}Cs atoms. In Section VI, we discuss the possibility of enhanced atom losses near dimer-dimer resonances.

II. FEW-BODY PHYSICS

In this section, we summarize the few-body physics that enters into our model for the avalanche mechanism. An avalanche is initiated by a 3-body recombination event in which three low-energy atoms collide to create an atom and a diatomic molecule, which can be either the shallow dimer or a deep dimer. The binding energy of the dimer is released in the kinetic energies of the outgoing atom and dimer. In the case of the deep dimer, the outgoing atom and dimer have very high energies and therefore small cross sections, so they escape from the trapping potential without any collisions. In the case of the shallow dimer, the outgoing atom and dimer have large cross sections, so they may undergo secondary collisions.

A. Few-body parameters

We consider identical bosons of mass m with a large positive scattering length a . The universal few-body reaction rates associated with the zero-range limit are determined by three parameters [1]:

- the scattering length a , which can be controlled experimentally by varying the magnetic field near a Feshbach resonance,
- the atom-dimer resonance a_* , or an equivalent Efimov parameter, upon which physical observables can only depend log-periodically,
- a dimensionless parameter η_* , which controls the decay width of an Efimov trimer.

The parameter η_* is nonzero only if there are deep dimers that provide decay channels for the Efimov trimer. The alkali atoms used in most cold atom experiments have many deep dimers.

In the negative- a region, the most dramatic loss features are a sequence of narrow peaks in the 3-body recombination rate at the 3-atom resonances $(e^{\pi/s_0})^n a_-$, where $e^{\pi/s_0} \approx 22.694$ is the discrete scaling factor, n is an integer, and a_- differs from a_* by a multiplicative constant:

$$a_- = -21.306 a_*. \quad (1)$$

The universal ratio a_-/a_* was obtained with 5 digits of accuracy by dividing a 5-digit result for $a_- \kappa_*$ calculated by Deltuva [13] by a 12-digit result for $a_* \kappa_*$ [1]. The parameters a_- and a_* related by Eq. (1) are the scattering lengths at which the same Efimov trimer crosses the 3-atom and atom-dimer thresholds. In the positive- a region, the most dramatic loss features are a sequence of minima in the 3-body recombination rate at $(e^{\pi/s_0})^n a_+$, where n is an integer and a_+ differs from a_* by a multiplicative constant:¹

$$a_+ = 4.4724 a_*. \quad (2)$$

The ratio $a_+/a_- = -e^{-\pi/2s_0}$ was obtained analytically by Hammer, Helfrich, and Petrov [14]. The ratio a_+/a_* in Eq. (2) is obtained by multiplying this analytic result by that in Eq. (1). Either a_- or a_+ can be used as the Efimov parameter in place of a_* . The ratios of the positions of loss features can differ from the universal ratios in Eqs. (1) and (2) due to nonuniversal effects associated with a nonzero range. Range corrections to the universal ratios have been analyzed by Ji, Phillips, and Platter [15].

B. Two-body observables

The 2-body physics that enters into our model for the avalanche mechanism consists of the binding energy for the shallow dimer and the cross section for atom-atom scattering.

¹ Some papers follow Ref. [6] in using a_+ to denote $e^{-\pi/2s_0} a_+ = 0.93882 a_*$. This is the position of a local maximum of L_3/a^4 but not of L_3 , where L_3 is the 3-body recombination rate constant. The parameter a_+ is preferable as an Efimov parameter because, in the limit $\eta_* \rightarrow 0$, it is the position of a zero of L_3 as well as L_3/a^4 . The resulting local minimum of L_3 is therefore a robust loss feature.

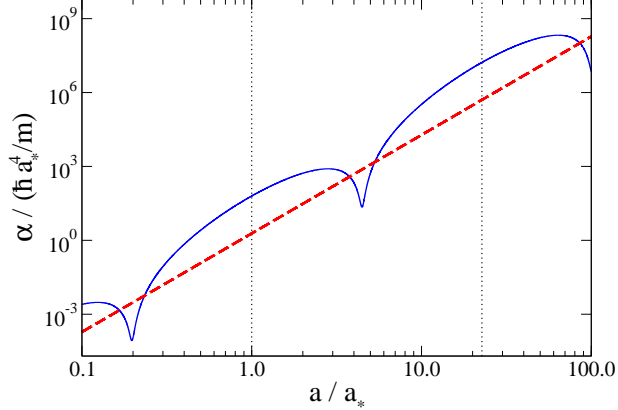


FIG. 1: (Color online) Universal rate constants for 3-body recombination at threshold for $\eta_* = 0.03$ as functions of the scattering length. The rate constant α_{shallow} for recombination into the shallow dimer is shown as a solid (blue) line. The rate constant α_{deep} for recombination into deep dimers is shown as a dashed (red) line that is almost straight. The vertical dotted lines mark the positions of a_* and $22.7 a_*$.

The universal binding energy for the shallow dimer is

$$E_d = \frac{\hbar^2}{ma^2}. \quad (3)$$

The universal cross section for the elastic scattering of a pair of identical bosonic atoms with center-of-mass wavenumber k_{cm} is

$$\sigma_{AA} = \frac{8\pi a^2}{1 + a^2 k_{\text{cm}}^2}. \quad (4)$$

This universal expression is accurate if k_{cm} is much smaller than the inverse range.

Three-body recombination at threshold creates an atom with wavenumber $k = 2/(\sqrt{3}a)$. The center-of-mass wavenumber for its first collision is $k_{\text{cm}} = 1/(\sqrt{3}a)$. In the elastic collision of an energetic atom with a stationary atom, the kinetic energy of either outgoing atom is smaller than that of the incoming atom by a factor whose average value is $1/2$. Thus the kinetic energies of the outgoing atoms decrease rapidly towards 0 as the avalanche develops. The decreasing kinetic energies imply increasing atom-atom cross sections, although the increase is not dramatic. If the recombination atom has many elastic collisions, its cross section is larger than for its first collision by a factor of about $4/3$.

C. Three-body recombination rates

The 3-body recombination event that initiates an avalanche either produces an atom and the shallow dimer or an atom and a deep dimer. We consider systems of atoms in which the energy per particle is much smaller than the binding energy E_d of the shallow dimer. We can therefore neglect the energies of the three incoming atoms and use the recombination rates at threshold. If the system of atoms has number density n , the recombination event rates can be expressed as αn^3 , where α is a rate constant. The universal event rate constants

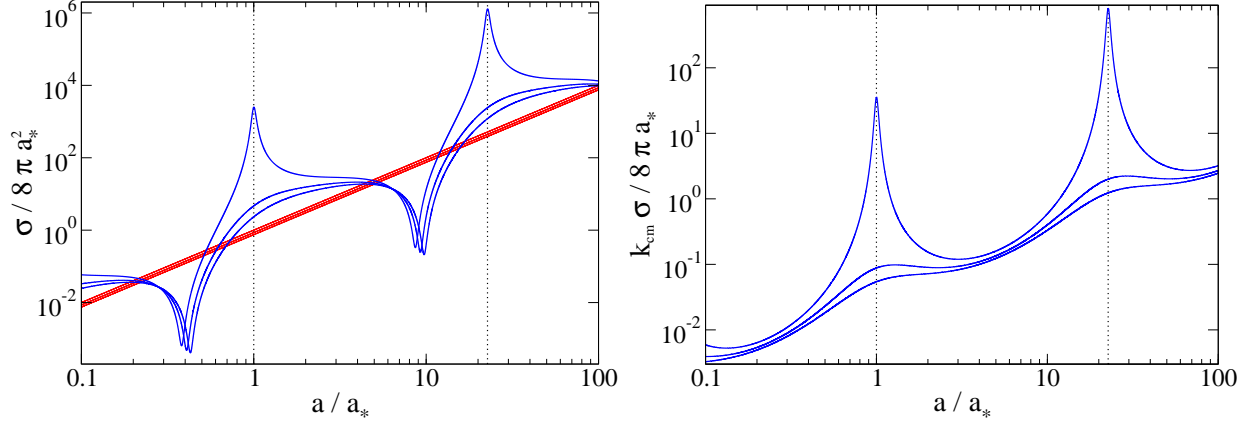


FIG. 2: (Color online) Universal cross sections $\sigma_{AD}^{(\text{el})}$ for elastic atom-dimer scattering (left panel) and $k_{\text{cm}}\sigma_{AD}^{(\text{in})}$ for inelastic atom-dimer scattering (right panel) for $\eta_* = 0.03$ as functions of the scattering length for three different energies. The vertical dotted lines mark the positions of a_* and $22.7 a_*$. The three curves (in order of increasing cross sections at $a = a_*$) are for the first scattering of the recombination dimer, a typical second scattering, and after many elastic scatterings. In the left panel, the three straight closely-spaced (red) lines are the corresponding elastic cross sections for atom-atom collisions.

α_{shallow} and α_{deep} for 3-body recombination at threshold into the shallow dimer and into deep dimers are conveniently expressed as functions of a , a_+ , and η_* [1]:

$$\alpha_{\text{shallow}} = \frac{128\pi^2(4\pi - 3\sqrt{3})(\sin^2[s_0 \ln(a/a_+)] + \sinh^2 \eta_*)}{\sinh^2(\pi s_0 + \eta_*) + \cos^2[s_0 \ln(a/a_+)]} \frac{\hbar a^4}{m}, \quad (5a)$$

$$\alpha_{\text{deep}} = \frac{128\pi^2(4\pi - 3\sqrt{3}) \coth(\pi s_0) \cosh \eta_* \sinh \eta_*}{\sinh^2(\pi s_0 + \eta_*) + \cos^2[s_0 \ln(a/a_+)]} \frac{\hbar a^4}{m}. \quad (5b)$$

These rate constants are shown as functions of a in Fig. 1 for $\eta_* = 0.03$. Both rate constants have log-periodic modulation of a^4 scaling behavior. For α_{shallow} , the log-periodic modulation produces local minima at scattering lengths near $(e^{\pi/s_0})^n a_+$ which become zeroes in the limit $\eta_* \rightarrow 0$. These minima arise from an Efimov interference effect. For α_{deep} , the amplitude of the log-periodic modulation is too small to be evident in Fig. 1.

D. Atom-dimer cross sections

The shallow dimer from 3-body recombination can collide with a low-energy atom in the cloud. Since the energy per particle in the atom cloud is much smaller than E_d , we neglect the energy of the atom and use the atom-dimer cross sections for a stationary atom. The collision between the shallow dimer and an atom can be elastic, in which case the diatomic molecule in the final state is the shallow dimer, or inelastic, in which case it is a deep dimer.

The energy dependence of the atom-dimer cross sections is important. In the collision of a dimer with wavenumber k with a stationary atom, the center-of-mass wavenumber k_{cm} is $k/3$. An avalanche is initiated by a recombination event at threshold creating an atom and a shallow dimer with wavenumbers $k = 2/(\sqrt{3}a)$. In the first collision of the dimer with a stationary atom, its center-of-mass wavenumber is $k_{\text{cm}} = 2/(3\sqrt{3}a)$. The collision energy

in the center-of-mass frame is $E_{\text{cm}} = \frac{1}{9}E_d$. A subsequent elastic collision with a stationary atom decreases the dimer's kinetic energy by a multiplicative factor whose average value is 5/9. As the number of elastic collisions of the dimer increases, E_{cm} decreases rapidly towards 0.

The universal elastic and inelastic atom-dimer cross sections $\sigma_{AD}^{(\text{el})}$ and $\sigma_{AD}^{(\text{in})}$ are conveniently expressed as functions of a , a_* , η_* , and the center-of-mass wavenumber k_{cm} . The S-wave elastic atom-dimer cross section is given by

$$\sigma_{AD}^{(\text{el})} = \frac{4\pi}{|k_{\text{cm}} \cot \delta_{AD}(k_{\text{cm}}) - ik_{\text{cm}}|^2}, \quad (6)$$

where $\delta_{AD}(k_{\text{cm}})$ is the S-wave phase shift. The total S-wave cross section can be expressed via the optical theorem as

$$\sigma_{AD}^{(\text{total})} = \frac{4\pi}{k_{\text{cm}}} \text{Im} \frac{1}{k_{\text{cm}} \cot \delta_{AD}(k_{\text{cm}}) - ik_{\text{cm}}}. \quad (7)$$

The S-wave inelastic cross section is obtained by subtracting the elastic cross section from the total cross section:

$$\sigma_{AD}^{(\text{in})} = \frac{4\pi}{k_{\text{cm}}} \frac{-\text{Im}[k_{\text{cm}} \cot \delta_{AD}(k_{\text{cm}})]}{|k_{\text{cm}} \cot \delta_{AD}(k_{\text{cm}}) - ik_{\text{cm}}|^2}. \quad (8)$$

Efimov's radial law strongly constraints the dependence of the phase shift on a_* [1], implying that it can be expressed as

$$ka \cot \delta_{AD}(k) = c_1(ka) + c_2(ka) \cot[s_0 \ln(a/a_*) + \phi(ka) + i\eta_*]. \quad (9)$$

The functions $c_1(ka)$, $c_2(ka)$, and $\phi(ka)$ have been determined from the atom-dimer threshold $k = 0$ to the dimer-breakup threshold $ka = 2/\sqrt{3}$ by calculating the phase shifts $\delta_{AD}(k)$ numerically using an effective field theory [1]. The results were parametrized as

$$c_1(ka) = -0.22 + 0.39(ka)^2 - 0.17(ka)^4, \quad (10a)$$

$$c_2(ka) = 0.32 + 0.82(ka)^2 - 0.14(ka)^4, \quad (10b)$$

$$\phi(ka) = -0.83(ka)^2 + 0.23(ka)^4. \quad (10c)$$

In the low-energy limit, the cross sections in Eqs. (6) and (8) are determined by the atom-dimer scattering length a_{AD} , which can be expressed in the form [1]

$$a_{AD} = (b_1 + b_2 \cot[s_0 \ln(a/a_*) + i\eta_*]) a, \quad (11)$$

where b_1 and b_2 are universal numerical constants: $b_1 \approx 1.46$, $b_2 \approx -2.15$. In the limit $\eta_* \rightarrow 0$, a_{AD} diverges at the atom-dimer resonance $a = a_*$. The low-energy limit of the elastic cross section is

$$\sigma_{AD}^{(\text{el})} \longrightarrow 4\pi |a_{AD}|^2. \quad (12)$$

The low-energy limit of the inelastic cross section multiplied by k_{cm} is

$$k_{\text{cm}} \sigma_{AD}^{(\text{in})} \longrightarrow 4\pi |a_{AD}|^2 \text{Im}(1/a_{AD}). \quad (13)$$

Both of the cross sections in Eqs. (12) and (13) have a factor of $\sin^2[s_0 \ln(a/a_*)] + \sinh^2 \eta_*$ in the denominator that produces a sharp peak at the atom-dimer resonance if $\eta_* \ll 1$.

The energy dependence of the universal atom-dimer cross sections is illustrated in Fig. 2. The elastic cross section $\sigma_{AD}^{(el)}$ and the inelastic cross section $k_{cm}\sigma_{AD}^{(in)}$ are shown as functions of a for $\eta_* = 0.03$ at three different energies. These energies correspond to the first collision of the recombination dimer ($E_{cm} = \frac{1}{9} E_d$), a typical second collision ($E_{cm} = \frac{5}{81} E_d$), and after many elastic collisions ($E_{cm} \rightarrow 0$). For the first collision, the elastic cross section has a broad peak as a function of a with a local maximum near $4.34 a_*$, which is close to the minimum in the 3-body recombination rate: $4.34 a_* \approx 0.97 a_+$. The inelastic cross section for the first collision increases monotonically with a . For the typical second collision of the recombination dimer, the elastic cross section is similar to that of the first collision, but the inelastic cross section has a broad maximum just above a_* . After many elastic collisions, both the elastic and inelastic atom-dimer cross sections peak sharply near a_* .

The atom-dimer cross sections in Eqs. (6) and (8) are the S-wave contributions only. There are also contributions from higher partial waves. In the universal zero-range limit, the higher partial wave contributions to the inelastic cross sections vanish and the higher partial wave contributions to the elastic cross sections are determined only by the scattering length a . The contribution from the L 'th partial wave has the threshold behavior $(E_{cm}/E_d)^L$. The leading contribution is P-wave, and it is suppressed by a factor of E_{cm}/E_d . Thus its contribution to the atom-dimer elastic cross section for the first collision of the recombination dimer ($E_{cm} = \frac{1}{9} E_d$) is expected to be about an order of magnitude smaller than the atom-atom cross section. In Fig. 2, the P-wave atom-dimer cross section would be given by a straight line that is parallel to but significantly lower than the lowest straight line for the atom-atom cross section. It would be completely negligible near an atom-dimer resonance at $a = a_*$, but it would decrease the depths of the minima in the cross section.

III. EXPERIMENTAL INPUTS

In this section, we summarize the experiments that have observed narrow loss features near an atom-dimer resonance. We identify the variables for these experiments that are required as inputs to our Monte Carlo model for the avalanche mechanism.

A. Loss features near the atom-dimer resonance

The first observation of a loss feature near an atom-dimer resonance was by a group at Innsbruck in 2008 [8]. They used a thermal gas that was a mixture of ^{133}Cs atoms and shallow dimers composed of those atoms. They observed peaks in the atom and dimer loss rates at a scattering length near $+400 a_0$. The peak arises from the resonant enhancement of the inelastic scattering of an atom and a shallow dimer into an atom and a deep dimer due to an Efimov trimer near the atom-dimer threshold. The Innsbruck group has also measured the loss rate for atom clouds consisting of ^{133}Cs atoms only. They did not observe any loss features near the atom-dimer resonance in systems with atoms only.

There are three experiments that have observed loss features near an atom-dimer resonance in atom clouds that do not contain dimers. The first such experiment was by a group at Florence in 2009 using both a BEC and a thermal gas of ^{39}K atoms [9]. They measured the 3-body loss rate constant L_3 as a function of the scattering length. They observed a

peak in L_3/a^4 near $-1500 a_0$ that can be attributed to an Efimov trimer near the 3-atom threshold. They also observed two local minima in L_3/a^4 near $+224 a_0$ and $+5650 a_0$ that can be attributed to successive Efimov interference minima. Of these three loss features, the highest precision in the determination of η_* was obtained from the local minimum near $224 a_0$. We therefore use this loss feature to determine the Efimov parameters: $a_+ = 224 a_0$ and $\eta_* = 0.043$. Given this value of a_+ and the universal ratio in Eq. (2), atom-dimer resonances are predicted near $50 a_0$ and $1140 a_0$. The Florence group observed enhancements in the loss rate near $+30.4 a_0$ in a BEC and near $+930 a_0$ in a thermal gas, both of which are reasonably close to the predicted atom-dimer resonances. They attributed these loss peaks to the avalanche mechanism of enhanced losses from secondary elastic collisions [9].

Another experiment in 2009 that observed a loss feature near an atom-dimer resonance was by a group at Rice University using both a BEC and a thermal gas of ^7Li atoms in the $|1, +1\rangle$ hyperfine state [10]. They observed two peaks in L_3/a^4 near $-298 a_0$ and near $-6301 a_0$ that can be attributed to successive Efimov trimers near the 3-atom threshold. They also observed two local minima in L_3/a^4 near $+119 a_0$ and $+2676 a_0$ that can be attributed to successive Efimov interference features. Of these four loss features, the highest precision in the determination of η_* was obtained from the local minimum near $2676 a_0$. We therefore use this loss feature to determine the Efimov parameters: $a_+ = 2676 a_0$ and $\eta_+ = 0.039$. Given this value of a_+ , an atom-dimer resonance is predicted at $598 a_0$. The Rice group observed an enhancement in L_3/a^4 in a BEC near $+608 a_0$, which is close to the predicted atom-dimer resonance.

The third experiment that observed a loss feature near an atom-dimer resonance in an atom cloud that contained no dimers was by a group at Bar-Ilan University using a thermal gas of ^7Li atoms in either the $|1, +1\rangle$ or $|1, 0\rangle$ hyperfine state [17]. For both hyperfine states, they observed a peak in L_3/a^4 near $-270 a_0$ that can be attributed to an Efimov trimer near the 3-atom threshold and a local minimum in L_3/a^4 near $+1170 a_0$ that can be attributed to Efimov interference. A more thorough analysis was presented in Ref. [18]. The Efimov parameters determined by fitting L_3 are $a_+ = 1260 a_0$ and $\eta_* = 0.188$. Given this value of a_+ , an atom-dimer resonance is predicted at $282 a_0$. In Ref. [11], additional data for a below $220 a_0$ were presented, revealing a narrow loss peak in L_3 near $+200 a_0$, which is reasonably close to the predicted atom-dimer resonance.

B. Experimental variables

The important experimental variables in the measurements of the loss rates of trapped atoms include the following:

- the frequencies ν_x , ν_y , and ν_z of the harmonic trapping potential, which has the form

$$V(x, y, z) = 2\pi^2 m (\nu_x^2 x^2 + \nu_y^2 y^2 + \nu_z^2 z^2). \quad (14)$$

- the initial number N_0 of trapped atoms.
- the temperature T of the atoms.
- the trap depth E_{trap} .
- the holding time t_{hold} , after which the remaining number N of trapped atoms is measured.

	${}^7\text{Li}$		${}^{39}\text{K}$		${}^{133}\text{Cs}$
	BEC [10]	thermal [18]	BEC [9]	thermal [9]	thermal [19]
ν_x	236.0 Hz	1300.0 Hz	75.0 Hz	75.0 Hz	16.6 Hz
ν_y	236.0 Hz	1300.0 Hz	75.0 Hz	75.0 Hz	18.31 Hz
ν_z	4.6 Hz	190.0 Hz	75.0 Hz	75.0 Hz	3.78 Hz
N_0	4.0×10^5	3.5×10^4	1.3×10^5	7.0×10^4	2.0×10^4
E_{trap}	0.5 μK	7 μK	1.0 μK	0.6 μK	0.2 μK
T	$< 0.105 \mu\text{K}$	1.4 μK	$< 0.17 \mu\text{K}$	0.1 μK	0.015 μK
t_{hold}	~ 0.003 s	0.01 – 5 s	1 s	0.17 s	~ 1 s
a	500 – 4000 a_0	159 – 2663 a_0	68 – 372 a_0	600 – 1548 a_0	35 – 1270 a_0

TABLE I: Experimental variables for experiments with ${}^7\text{Li}$, ${}^{39}\text{K}$, and ${}^{133}\text{Cs}$ atoms: the trapping frequencies ν_x , ν_y , and ν_z , the initial number of atoms N_0 , the trap depth E_{trap} , the temperature T , the holding time t_{hold} , and the range of scattering lengths a . In the case of a BEC, we give only an upper bound on the temperature T . The upper bound is $\frac{1}{2}T_c$ for the BEC in Ref. [10] and T_c for the thermal gas in Ref. [9].

In Table I, we list the important experimental variables for five experiments with ${}^7\text{Li}$ atoms [10, 18], ${}^{39}\text{K}$ atoms [9], and ${}^{133}\text{Cs}$ atoms [19]. In two of the 5 experiments, the atom cloud was a BEC and in the other three, it was a thermal gas. The experimental variables that are not given explicitly in the references were obtained from private communications with the authors. Different values of the experimental variables were used in different regions of the scattering length. The values listed in Table I are those that were used in the range of a given in the Table.

The holding time t_{hold} is generally chosen to be large enough that a significant fraction of the initial number N_0 of atoms are lost, so that this fraction can be measured with some precision. The product of t_{hold} and a trapping frequency gives the number of periods of the oscillation in that dimension before the atom number is measured. The holding time is not used as an input in the Monte Carlo model for simulating avalanches described in Section IV.

We use a simple model for the trap depth that is specified by the single variable E_{trap} . Atoms and dimers that reach the edge of the atom cloud are assumed to be lost if their kinetic energies exceed E_{trap} and $2E_{\text{trap}}$, respectively. Equivalently, this model for the trap depth can be expressed as a modification of the trapping potential for the atoms. The potential for a single atom is given by Eq. (14) if $V(x, y, z) < E_{\text{trap}}$ and is equal to the constant E_{trap} if $V(x, y, z) > E_{\text{trap}}$. The trap depth E_{trap} is generally substantially larger than the energy per atom E/N .

The number of atoms lost also depends on the dimer binding energy $E_d = \hbar^2/ma^2$, which depends on the scattering length. If $E_d < \frac{3}{2}E_{\text{trap}}$, the recombination atom and the recombination dimer both remain trapped. The dimer will eventually scatter inelastically from an atom in the cloud, so the number of lost atoms is 3. If $\frac{3}{2}E_{\text{trap}} < E_d < 6E_{\text{trap}}$, the recombination dimer is trapped and must ultimately scatter inelastically, but the recombination atom is not trapped. The largest possible number of lost atoms in the avalanche initiated by the recombination atom is the integer part of $(2/3)E_d/E_{\text{trap}}$, which can be 1, 2, or 3, depending on a . The dimer could also produce a single lost atom through an elastic collision, and it will eventually suffer an inelastic collision, resulting in the loss of 3 more atoms. Thus the

maximum number of lost atoms increases from 3 to 7 as E_d increases from $\frac{3}{2}E_{\text{trap}}$ to $6E_{\text{trap}}$. If $E_d > 6E_{\text{trap}}$, neither the atom nor the shallow dimer is trapped, so N_{lost} can be as large as $E_d/E_{\text{trap}} + 3$. Our simple model for the trap depth implies discontinuities in physical observables at $E_d = \frac{3}{2}E_{\text{trap}}$ and $E_d = 6E_{\text{trap}}$. Thus a more elaborate model is probably required to give accurate predictions for the number of lost atoms in a region that includes the interval $\frac{3}{2}E_{\text{trap}} < E_d < 6E_{\text{trap}}$.

C. Number densities

The frequencies ν_x , ν_y , and ν_z , the initial number N_0 of trapped atoms, and the temperature T determine the number density $n(x, y, z)$ of the atoms. We consider three simple cases for the system of trapped atoms:

- a Bose-Einstein condensate (BEC) of atoms at 0 temperature in the Thomas-Fermi limit,
- a thermal gas of atoms in the weak-interaction limit at the critical temperature T_c ,
- a thermal gas of atoms in the weak-interaction limit at a temperature T much larger than T_c .

In a BEC of atoms at zero temperature in the Thomas-Fermi limit, the number density depends on the scattering length a :

$$n(x, y, z) = \frac{m}{4\pi\hbar^2 a} \max\{\mu(a) - V(x, y, z), 0\}, \quad (15)$$

where $\mu(a)$ is the chemical potential, which also depends on a :

$$\mu(a) = \frac{\hbar^2}{2m} \left(\frac{15Na}{a_x^2 a_y^2 a_z^2} \right)^{2/5}. \quad (16)$$

The trap lengths a_x , a_y , and a_z are determined by the trapping frequencies: $a_i = (\hbar/2\pi m\nu_i)^{1/2}$. The energy per atom is just the chemical potential:

$$E/N = \mu(a). \quad (17)$$

The critical temperature for Bose-Einstein condensation in the trapping potential is

$$k_B T_c = \frac{\hbar^2}{m} \left(\frac{N}{\zeta(3) a_x^2 a_y^2 a_z^2} \right)^{1/3}, \quad (18)$$

where $\zeta(3) \approx 1.202$. For a thermal cloud of trapped atoms above T_c , the appropriate phase-space distribution in the weak-interaction limit is the Bose-Einstein distribution. At the critical temperature, the number density can be expressed in terms of a polylogarithm:

$$n(x, y, z) = \left(\frac{mk_B T_c}{2\pi\hbar^2} \right)^{3/2} \text{Li}_{3/2}(\exp(-V(x, y, z)/k_B T_c)). \quad (19)$$

The energy per atom at T_c is

$$E/N = \frac{\pi^4}{30\zeta(3)} k_B T_c, \quad (20)$$

which is approximately $2.7012 k_B T_c$.

If T is large enough compared to T_c , the Bose-Einstein distribution can be approximated by the Boltzmann distribution. The number density then reduces to a Gaussian:

$$n(x, y, z) = \frac{N\lambda_T^3}{8\pi^3 a_x^2 a_y^2 a_z^2} \exp(-V(x, y, z)/k_B T), \quad (21)$$

where $\lambda_T = (2\pi\hbar^2/mk_B T)^{1/2}$ is the thermal quantum wavelength. The energy per atom is given by the equipartition theorem:

$$E/N = 3k_B T. \quad (22)$$

D. Loss rate and heating rate

The rate at which the local number density $n(\mathbf{r})$ of atoms in a thermal gas decreases due to 3-body recombination can be expressed as a local differential equation:

$$\frac{d}{dt}n(\mathbf{r}) = -(N_{\text{lost}}(\mathbf{r})\alpha_{\text{shallow}} + 3\alpha_{\text{deep}})n^3(\mathbf{r}), \quad (23)$$

where $N_{\text{lost}}(\mathbf{r})$ is the average number of atoms lost from a recombination event that creates a shallow dimer at the point \mathbf{r} . Upon integrating Eq. (23) over space, we obtain the rate at which the number N of atoms decreases:

$$\frac{dN}{dt} = -(\langle N_{\text{lost}} \rangle \alpha_{\text{shallow}} + 3\alpha_{\text{deep}}) \langle n^2 \rangle N, \quad (24)$$

where $\langle n^2 \rangle$ and $\langle N_{\text{lost}} \rangle$ are spacial averages weighted by $n(\mathbf{r})$ and $n^3(\mathbf{r})$, respectively. Equivalently, $\langle N_{\text{lost}} \rangle$ is the number of atoms lost in a single avalanche averaged over the probability distribution for avalanches. In the case of a BEC, the right sides of Eqs. (23) and (24) should be multiplied by $1/6$ to take into account that the 3 atoms undergoing recombination are identical bosons. The loss rate constant L_3 is defined to be the coefficient of $-\langle n^2 \rangle N$ in dN/dt for thermal gas:

$$L_3 = \langle N_{\text{lost}} \rangle \alpha_{\text{shallow}} + 3\alpha_{\text{deep}}. \quad (25)$$

Measurements of L_3 in a BEC and in a thermal gas of the same atoms should agree to within experimental uncertainties.

Atoms in the avalanche with kinetic energy less than E_{trap} can never escape from the trapping potential. Through subsequent elastic collisions, their kinetic energy is ultimately transformed into heat. If most of the heat is deposited near the recombination point, the rate at which a thermal gas of trapped atoms gains heat Q from the avalanche mechanism is

$$\frac{dQ}{dt} = \langle E_{\text{heat}} \rangle \alpha_{\text{shallow}} \langle n^2 \rangle N, \quad (26)$$

where $\langle E_{\text{heat}} \rangle$ is the average amount of energy transformed into heat in a single avalanche. In the case of a BEC, the right side of Eqs. (26) should be multiplied by $1/6$ to take into account that the 3 atoms undergoing recombination are identical bosons.

The number density profiles in Eq. (15) for a BEC and in Eq. (21) for a thermal gas are those that would be expected in the absence of atom loss processes, such as 3-body recombination. Loss processes decrease the number N of atoms, allow energy to be carried out of the system by the lost atoms, and also add heat Q to the system. These effects can change the number density and the energy density of atoms as functions of time. In the case of a BEC, the atom loss and heating can generate a thermal cloud inside and surrounding the BEC. If too much energy is added to the system, its temperature can be raised above the critical temperature for Bose-Einstein condensation, in which case the BEC component disappears completely.

In the case of a thermal gas, the atom loss and the heating change the number of atoms N and their total energy. If the thermalization rate is sufficiently fast, the number density can still be approximated by the density profile in Eq. (21) with time-dependent N and T . To measure the loss rate constant L_3 , that time dependence must be taken into account. A method for doing this was developed in Ref. [22]. The coupled rate equations for N and T (in the absence of background gas collisions) were expressed in the form

$$\frac{dN}{dt} = -\frac{\gamma N^3}{T^3}, \quad (27a)$$

$$\frac{dT}{dt} = \frac{\gamma(T + T_h)N^2}{3T^3}, \quad (27b)$$

where γ and T_h are constants. The solutions to these coupled differential equations depend on γ and T_h . If $N(t)$ is measured as a function of the holding time t , the two parameters can be adjusted to fit that time dependence. The rate constant L_3 can then be determined from the fitted value of γ :

$$L_3 = \left(\frac{\sqrt{3}k}{2\pi m\bar{\nu}^2} \right)^3 \gamma, \quad (28)$$

where $\bar{\nu} = (\nu_x\nu_y\nu_z)^{1/3}$ is the geometric mean of the trapping frequencies.

We can derive the coupled equations for N and T in Eqs. (27) from our rate equations for N and Q in Eqs. (24) and (26). This derivation determines the fitting parameters γ and T_h in terms of the quantities $\langle N_{\text{lost}} \rangle$ and $\langle E_{\text{heat}} \rangle$ associated with the avalanche mechanism. The total energy E of the thermal gas in a harmonic trap is $E = 3Nk_B T$. It changes because the recombination event delivers energy to an atom and a dimer, the lost atoms carry away their kinetic energy, and the atoms that are elastically scattered but remain trapped deposit their energy as heat. The average energy of an atom in the thermal cloud is $3k_B T$. Since the recombination probability is proportional to $n^3(x, y, z)$, the incoming atoms in a 3-body recombination event have a smaller average energy $2k_B T$. If all the lost atoms originate near the recombination point, their average energy is also $2k_B T$. Thus the rate of change in the total energy is

$$\frac{dE}{dt} = -(\langle N_{\text{lost}} \rangle \alpha_{\text{shallow}} + 3\alpha_{\text{deep}}) \langle n^2 \rangle N(2k_B T) + \frac{dQ}{dt}. \quad (29)$$

Setting $E = 3Nk_B T$ and using Eqs. (24) and (26) for dN/dt and dQ/dt , we can obtain a rate equation for T :

$$\frac{dT}{dt} = \left(\frac{\alpha_{\text{shallow}} \langle E_{\text{heat}} \rangle}{3k_B T} + \frac{\langle N_{\text{lost}} \rangle \alpha_{\text{shallow}} + 3\alpha_{\text{deep}}}{3} \right) \langle n^2 \rangle T. \quad (30)$$

The density-weighted average $\langle n^2 \rangle$ in a thermal gas is

$$\langle n^2 \rangle = \frac{1}{3\sqrt{3}} \left(\frac{N\lambda_T^3}{8\pi^3 a_x^2 a_y^2 a_z^2} \right)^2. \quad (31)$$

Since this is proportional to N^2/T^3 , the rate equations for N in Eq. (24) and T in Eq. (30) do have the form given in Eqs. (27). The constant γ is proportional to the rate constant L_3 in Eq. (25) in accord with Eq. (25). The product of the constants γ and T_h in Eq. (27b) is determined by $\langle E_{\text{heat}} \rangle$ only:

$$\gamma T_h = \left(\frac{2\pi m \bar{v}^2}{\sqrt{3}k} \right)^3 \frac{\alpha_{\text{shallow}} \langle E_{\text{heat}} \rangle}{k}. \quad (32)$$

In Ref. [22], $k_B T_h$ was interpreted as the energy per lost atom. Combining Eqs. (32) and (28) with the expression for L_3 in Eq. (25), we see that $k_B T_h$ is indeed equal to E_{heat} if α_{deep} is negligible compared to α_{shallow} .

In Section IV, we develop a Monte Carlo model for the avalanche mechanism that can be used to calculate N_{lost} and E_{heat} . These quantities can also be determined experimentally using the values of γ and T_h obtained by fitting the time dependence of $N(t)$. By comparing the calculated and measured values of N_{lost} and E_{heat} , we could test our Monte Carlo model for the avalanche mechanism and perhaps develop a more accurate description of the loss process.

IV. MONTE CARLO METHOD

In this section, we describe our Monte Carlo model for the avalanche mechanism. We also compare it to previous models for the avalanche mechanism.

A. Approximations

The important energy scales in cold atom experiments include the energy per atom E/N , the trap depth E_{trap} , and the dimer binding energy $E_d = \hbar^2/m a^2$, which depends on the scattering length a . For a thermal gas with temperature T , E/N is $3k_B T$. For a BEC, E/N is equal to the chemical potential $\mu(a)$ given in Eq. (16), which depends on a . Another relevant energy scale is $2.7 k_B T_c$, which is the energy per atom at the critical temperature. In the case of a thermal gas, E/N must be significantly larger than $2.7 k_B T_c$ in order to use the Boltzmann distribution instead of the Bose-Einstein distribution. In the case of a BEC, $N(2.7 k_B T_c)$ is roughly the heat energy that must be added to change it to a thermal gas. The various energy scales are listed in Table II for each of the five sets of experimental variables listed in Table I.

Our simple model for the trap depth is described in Section III B. If an energetic atom or dimer reaches the edge of the cloud, it is lost from the trap if its kinetic energy is greater than E_{trap} or $2E_{\text{trap}}$, respectively. Otherwise it will follow a curved trajectory that returns to the cloud. A trapped atom that returns to the cloud will eventually thermalize through elastic collisions, transforming its kinetic energy into heat. A trapped dimer that returns to the atom cloud will eventually suffer an inelastic collision that results in the loss of 3 atoms.

	${}^7\text{Li}$		${}^{39}\text{K}$		${}^{133}\text{Cs}$
	BEC [10]	thermal [18]	BEC [9]	thermal [9]	thermal [19]
E/N	0.10 – 0.23	4.2	0.049 – 0.10	0.3	0.045
$2.7 k_B T_c$	0.57	2.7	0.46	0.38	0.035
E_{trap}	0.5	7	1.0	0.6	0.2
E_d	100 – 1.5	980 – 3.5	960 – 32	12 – 1.9	1040 – 0.81

TABLE II: Energy scales in μK for experiments with ${}^7\text{Li}$, ${}^{39}\text{K}$, and ${}^{133}\text{Cs}$ atoms: the energy per atom E/N , the energy per atom at the critical temperature $2.7 k_B T_c$, the trap depth E_{trap} , and the range of the dimer binding energy $E_d = \hbar^2/ma^2$. The ranges of E/N for a BEC and the ranges of E_d correspond to the ranges of a given in Table I.

Before the inelastic collision, it could scatter elastically, transforming some of its kinetic energy into heat, but we ignore that small contribution to the heat.

The trap depth E_{trap} is usually substantially larger than the energy per particle E/N . Otherwise, atoms will be rapidly lost from the trap until most of the atoms have energy smaller than E_{trap} . The energy per particle is more than an order of magnitude smaller than E_{trap} over most of the range of scattering length for most of the experiments listed in Table I. The exceptions are the ${}^7\text{Li}$ BEC experiment at the upper end of the range of a , where E/N is about $0.5 E_{\text{trap}}$ and the ${}^7\text{Li}$ and ${}^{39}\text{K}$ thermal gas experiments, in which E/N is also about $0.5 E_{\text{trap}}$. In these cases, our simple model for the trap depth may not be sufficient to calculate the effects of the avalanche mechanism accurately.

As a is increased by adjusting the magnetic field, the dimer binding energy E_d can decrease from much larger than E_{trap} to much smaller than E_{trap} . However it usually remains much larger than E/N . This allows the kinetic energies of the atoms in the cloud to be ignored in few-body reaction rates. For the experiments listed in Table I, E_d is more than an order of magnitude larger than E/N over most of the range of scattering lengths. There are a few exceptions near the upper ends of the ranges of a . In the ${}^7\text{Li}$ BEC experiment and the ${}^{39}\text{K}$ thermal gas experiment, E_d becomes as small as $6 E/N$ at the largest values of a . In the ${}^7\text{Li}$ thermal gas experiment, E_d becomes as small as $0.8 E/N$ at the largest value of a .

If the atom cloud is a BEC in the Thomas-Fermi limit, the trajectory of an energetic atom inside the BEC is a straight line, because the trapping potential energy of an atom and its mean-field energy add up to the constant chemical potential $\mu(a)$. If the atom flies beyond the edge of the BEC, it follows a curved trajectory determined by the harmonic potential. The trajectory of an energetic dimer is curved even inside the BEC, because its mean-field energy differs from that of a pair of atoms. If the atoms are in a thermal cloud, the trajectory of an energetic atom or energetic dimer is always curved. However if the kinetic energy of the atom or dimer is large enough that it can transfer an energy greater than E_{trap} to an atom in the cloud through an elastic collision, its trajectory has small curvature, and it can be approximated by a straight line. The kinetic energy of an atom or the dimer can change between scattering points, because the potential energy (and, in the case of a BEC, the mean-field energy) depends on the position in the cloud. However if the kinetic energy of the atom or dimer is large enough that it can transfer an energy greater than E_{trap} to an atom in the cloud, the change in the kinetic energy is negligible.

The rate equations for N and Q in Eqs. (24) and (26) were derived from the local rate equation for $n(\mathbf{r})$ in Eq. (23). However the avalanche mechanism makes the loss process

partly nonlocal. Some of the atoms that escape from the trapping potential receive their kinetic energy from an elastic collision at a scattering point (x, y, z) that may not be near the recombination point (x_0, y_0, z_0) . The distance $[(x - x_0)^2 + (y - y_0)^2 + (z - z_0)^2]^{1/2}$ is not a good measure of the nonlocality, because the length scales set by the trapping potential are different in different directions. A better measure of the nonlocality is the dimensionless distance

$$\hat{\ell}^2 = \frac{(x - x_0)^2}{a_x^2} + \frac{(y - y_0)^2}{a_y^2} + \frac{(z - z_0)^2}{a_z^2}. \quad (33)$$

which is the square of the number of oscillator lengths separating the recombination point and the scattering point. The local approximation for the loss rate will be valid if $\langle \hat{\ell}^2 \rangle \ll 1$, where the average is over lost atoms and over avalanches. If there are no collisions, the scattering point coincides with the recombination point and $\hat{\ell}^2 = 0$. In general, $\langle \hat{\ell}^2 \rangle$ depends on the prescription for the average. Since the atoms are identical bosons, a lost atom could be identified with any of the stationary atoms in the chain of previous elastic scatterings or with one of the three incoming atoms in the recombination event. Thus the scattering point (x, y, z) for a lost atom can be taken as its point of last scattering or the recombination point or any of the collision points in between. The atoms composing a dimer that escapes or scatters inelastically could be identified with two of the incoming atoms in the recombination event, but they also could be identified with any of the stationary atoms from which the dimer scattered elastically. One possible prescription is to choose the scattering point (x, y, z) to be the first collision point for any of its ancestors in the binary tree with equal probability. A more reasonable prescription is to choose the scattering point (x, y, z) to be the collision point at which the greatest energy is imparted to the lost atom or to one of its ancestors. With this prescription, the 3 lost atoms from an inelastic atom-dimer collision will be assumed to come from the inelastic collision point. For those atoms that are lost individually, the most energetic will be assumed to come from the recombination point with $\hat{\ell}^2 = 0$. The other lost atoms will usually be assumed to come from one of the first elastic collisions after the recombination event. This prescription is likely to give $\langle \hat{\ell}^2 \rangle \ll 1$, thus providing some justification for the local approximation.

We now list the most important approximations made in our Monte Carlo model:

- We neglect the energies of the low-energy atoms in the atom cloud.
- We approximate the trajectories of the dimer and the atoms between scattering events by straight lines.
- We take the momentum of an incoming atom or dimer in a collision to be the same as that particle's outgoing momentum from the previous scattering event.
- When comparing the energy of an atom or dimer to the trap depth, we ignore its potential energy (and, in the case of a BEC, its mean-field energy).
- We make the local approximation that most of the lost atoms come from near the recombination point and also that most of the heat from scattered atoms that are not lost is deposited near the recombination point.

B. Simulating avalanches

The development of an avalanche can be decomposed into discrete steps corresponding to the recombination event and the subsequent scattering events. Given the state of the avalanche immediately before each event, the state immediately after the event has a simple probability distribution. All these simple probability distributions together determine the probability distribution of avalanches. We can generate avalanches with this probability distribution using a Monte Carlo method. At each of the events in the evolution of the avalanche, we use a random number generator to determine the subsequent state. The simple probability distributions can be generated as follows:

- The position (x, y, z) of the recombination point, whose probability distribution is proportional to $n^3(x, y, z)$, is determined by three random numbers.
- The outgoing wavevectors \mathbf{k} and \mathbf{k}' for a pair of scattered particles are determined by the incoming wavevectors and two random numbers. In the center-of-momentum frame, the distribution of the wavevectors $\pm\mathbf{k}_{\text{cm}}$ is isotropic.
- Whether or not an atom or dimer produced by the recombination event or a scattering event is scattered before it reaches the edge of the atom cloud is determined by whether the scattering probability $1 - \exp(-\sigma \int n \, dl)$ is greater than or less than a random number between 0 and 1. The cross section σ is σ_{AA} if the particle is an atom and $\sigma_{AD}^{(\text{el})} + \sigma_{AD}^{(\text{in})}$ if it is a dimer. The column density $\int n \, dl$ is calculated by integrating from the position of the recombination or scattering event out to infinity along a straight line in the direction of the wavevector \mathbf{k} of the particle. If the atom or dimer scatters, the same random number is used to determine the position of its scattering event by solving for the length ℓ along the path for which $1 - \exp(-\sigma \int_0^\ell n \, dl)$ is equal to the random number.
- Given that a dimer scatters, it scatters inelastically if the probability $\sigma_{AD}^{(\text{in})}/(\sigma_{AD}^{(\text{el})} + \sigma_{AD}^{(\text{in})})$ is greater than a random number between 0 and 1. Otherwise, the dimer scatters elastically.

C. Atom loss and heating

The Monte Carlo method described in Section IV B generates a binary tree. The initial node, which represents the recombination event, has two branches corresponding to the dimer and the atom. For every elastic scattering event, there is a node with two branches that correspond to the two outgoing particles. Finally there are terminal nodes associated with atoms or dimers whose ultimate fate has been determined. More specifically, the terminal nodes correspond to atoms or dimers that are lost, atoms or dimers that are trapped, and dimers that have inelastic collisions. Each terminal node gives a contribution ΔN_{lost} to the number of atoms lost and ΔE_{heat} to the heat of the remaining atoms. The conditions for a branch to end at a terminal node and the corresponding values of ΔN_{lost} and ΔE_{heat} are as follows:

- If an outgoing atom from a scattering event has kinetic energy $E < E_{\text{trap}}$, it remains trapped: $\Delta N_{\text{lost}} = 0$ and $\Delta E_{\text{heat}} = E$.

- If an atom that reaches the edge of the atom cloud has kinetic energy $E > E_{\text{trap}}$, it is lost: $\Delta N_{\text{lost}} = 1$ and $\Delta E_{\text{heat}} = 0$.
- If a dimer has an inelastic collision, both it and the scattered atom are lost: $\Delta N_{\text{lost}} = 3$ and $\Delta E_{\text{heat}} = 0$.
- If a dimer that reaches the edge of the atom cloud has kinetic energy $E > 2E_{\text{trap}}$, it is lost: $\Delta N_{\text{lost}} = 2$ and $\Delta E_{\text{heat}} = 0$.
- If a dimer that reaches the edge of the atom cloud has kinetic energy $E < 2E_{\text{trap}}$, it will return to the cloud and will eventually suffer an inelastic collision: $\Delta N_{\text{lost}} = 3$ and $\Delta E_{\text{heat}} = 0$. We ignore any heat from additional elastic collisions before the final inelastic collision.

The number of terminal nodes in the binary tree is 2 if the cross section and the column density are small enough that there is no scattering. The number of terminal nodes is generally larger in a BEC than in a thermal gas. For the sets of experimental variables listed in Table I, the number of terminal nodes is sometimes greater than 50.

The quantities N_{lost} and E_{heat} for a single avalanche are obtained by adding up ΔN_{lost} and ΔE_{heat} for all the terminal nodes. Their averages $\langle N_{\text{lost}} \rangle$ and $\langle E_{\text{heat}} \rangle$ are calculated by averaging over many avalanches generated using the Monte Carlo method described in Section IV B. These averages have discontinuities as functions of a at $E_d = \frac{3}{2}E_{\text{trap}}$ and $E_d = 6E_{\text{trap}}$, which are artifacts of our simple model for the trap depth. Aside from these two points, $\langle N_{\text{lost}} \rangle$ and $\langle E_{\text{heat}} \rangle$ are smooth functions of a . The number of avalanches required to get smooth results is particularly large in the region near the interval $\frac{3}{2}E_{\text{trap}} < E_d < 6E_{\text{trap}}$ in which the recombination dimer is trapped but the recombination atom is not. More than 100,000 avalanches are sometimes required to get smooth results in this region.

D. Previous models

Zaccanti et al. developed a simple probabilistic model for the avalanche process that we will refer to as the *Zaccanti model* [9]. In the Zaccanti model, the avalanche is reduced to a discrete sequence of dimer scattering events. A variable number of elastic collisions is followed either by the escape of the dimer from the trap or by a final inelastic collision. There is one lost atom for each elastic collision up to a maximum number that is determined by the trap depth E_{trap} . The relative probability for each sequence of scattering events is determined by the mean column density $\langle \int n d\ell \rangle$ of the trapped atoms and by the atom-dimer cross sections $\sigma_{AD}^{(\text{el})}$ and $\sigma_{AD}^{(\text{in})}$. The Zaccanti model is greatly simplified in several ways compared to our Monte Carlo model:

- The energy dependence of $\sigma_{AD}^{(\text{el})}$ and $k_{\text{cm}}\sigma_{AD}^{(\text{in})}$ is not taken into account. These cross sections were approximated by their low-energy limits given in Eqs. (12) and (13), which correspond with the sharply-peaked cross sections in Fig. 2.
- The spacial structure of the avalanche is ignored. All 3-body recombination events occur at the center of the cloud. The scattering probabilities are all determined by the mean column density $\langle \int n d\ell \rangle$ averaged over directions from the center of the trap.

- The elastic scattering of the atoms is not considered. The atom from the recombination event and the scattered atoms from elastic atom-dimer collisions cannot become trapped by losing energy and they also cannot initiate avalanches of additional lost atoms.
- The random variations associated with S-wave scattering are not taken into account. Each elastic collision decreases the kinetic energy of the dimer by the same multiplicative factor $5/9$.

Zaccanti et al. used their model to calculate the average number $\langle N_{\text{lost}} \rangle$ of lost atoms for their experiment with ^{39}K atoms [9]. It predicts that $\langle N_{\text{lost}} \rangle$ increases from its background value of 3 to about 13 near the atom-dimer resonance. The resulting prediction for the atom loss rate agreed qualitatively with the loss feature they observed near $30.4 a_0$. The agreement could be made quantitative by decreasing $\sigma_{AD}^{(\text{el})}$ by a factor of 30. Such a decrease was motivated by the energy dependence of the elastic atom-dimer cross section.

Machtey et al. developed an alternative probabilistic model for the avalanche process in Ref. [20]. They made the same simplifications that were itemized above for the Zaccanti model. They reduced the avalanche to discrete sequences of dimer scattering events whose probabilities are determined by an effective column density and the atom-dimer cross sections, but their probabilities for the sequences of scattering events were different from the Zaccanti model. Another difference was that Machtey et al. never introduced the trap depth E_{trap} into their model. As a consequence, they could not calculate $\langle N_{\text{lost}} \rangle$. Instead they used their model to calculate the average number \bar{N} of dimer collisions, which is not observable. Machtey et al. suggested that the maximum of \bar{N} as a function of a might coincide with a local maximum of the atom loss rate.

E. Improvements in the Model

Our Monte Carlo model for the avalanche mechanism has several significant improvements over the probabilistic models proposed by Zaccanti et al. [9] and by Machtey et al. [20]. There are a number of further improvements that could be made. The approximations made in our Monte Carlo model are itemized at the end of Section IV A. Many of them involve neglecting the energies of the low-energy atoms in the atom cloud. One of these approximations is that the energies of the atoms that undergo 3-body recombination are much less than E_d . This allowed us to use the universal rate constants at threshold α_{shallow} and α_{deep} in Eqs. (5). This approximation could be removed for a thermal gas by using the universal results for the 3-body recombination rates in Ref. [21], which were calculated up to temperatures about 100 times larger than E_d . The other low-energy approximations allowed the trajectories of particles between collisions to be approximated by straight lines and the changes in their kinetic energies between collisions to be ignored. If the potential energies of the atoms and the dimer (and, in the case of a BEC, their mean-field energies) are taken into account, their trajectories become curved and their kinetic energies change between collisions in accord with conservation of energy. These improvements would be straightforward to implement in our Monte Carlo model.

Another approximation is that we used a simple model for the trap depth that can be expressed as a change in the trapping potential with a single parameter E_{trap} . The physics represented by that trap depth is actually much more complicated. Given our simple model

for the trap depth, it is not clear that the improvement in accuracy from eliminating the low-energy approximations would be worth the effort.

Finally, our rate equations for N and Q in Eqs. (24) and (26) are based on the local rate equation for the number density in Eq. (23). At each collision point in the avalanche, a low-energy atom is replaced by a high-energy atom that can then propagate through the atom cloud. The local approximation requires that most of the lost atoms come from near the recombination point and also that most of the heat from the scattered atoms that are not lost is deposited near the recombination point. Removing this local approximation would be an enormous complication.

V. RESULTS

In this section, we apply our Monte Carlo model for the avalanche mechanism to the experiments with ^{39}K and ^7Li atoms in which narrow loss peaks near an atom-dimer resonance have been observed. We also apply it to an experiment with ^{133}Cs atoms in which such a loss feature has not been observed.

A. ^{39}K atoms

In 2009, the Florence group observed peaks in L_3/a^4 near $30.4 a_0$ in a BEC of ^{39}K atoms and near $930 a_0$ in a thermal gas of ^{39}K atoms [9]. Both loss features were near the predicted position of an atom-dimer resonance. Since the van der Waals length for ^{39}K atoms is $139 a_0$, the loss feature near $30.4 a_0$ is in a nonuniversal region of small scattering length. We therefore focus on larger scattering lengths that are safely in the universal region. Different experimental variables were used in different regions of the scattering length. We consider the experimental variables used in the two regions listed in Table I. In one region, the atom cloud was a BEC and in the other region, it was a thermal gas. We choose the Efimov parameters that were determined from the local minimum of L_3/a^4 near $224 a_0$: $a_* = 1140 a_0$ and $\eta_* = 0.043$. For the thermal gas experiment, $E/N = 3k_B T$ in Table II is actually smaller than the value of $2.7 k_B T_c$ calculated from N . This suggests that the system is very close to the critical temperature, so it might be appropriate to use the number density in Eq. (19). We nevertheless use the Boltzmann approximation in Eq. (21) for simplicity.

In the left panels of Fig. 3, the average number N_{lost} of atoms lost and the average heat E_{heat} from the avalanche are shown as functions of a for the two sets of experimental variables for ^{39}K atoms listed in Table I. (In this section, we omit the angular brackets that denote the avalanche averages of N_{lost} and E_{heat} .) For both the BEC and the thermal gas, N_{lost} and E_{heat} are shown for a range of scattering lengths that extend over two orders of magnitude. The rate constant L_3 however was measured using these experimental variables only over the smaller ranges of a specified in Table I. For both the BEC and the thermal gas, N_{lost} has a broad peak with a maximum value near 5. The position of the peak is at $293 a_0$ for the BEC and at $827 a_0$ for the thermal gas. This position is determined by the atom-dimer cross sections and the trap depth, among other things. As illustrated in Fig. 2, the cross section for the first elastic scattering of the recombination dimer has a broad peak with maximum at $4.34(e^{-\pi/s_0} a_*) \approx 218 a_0$. The trap depth forces N_{lost} to decrease to the naive value 3 when $E_d = \frac{3}{2} E_{\text{trap}}$, which is near $a = 1720 a_0$ for the BEC and near $a = 2220 a_0$ for the thermal gas. Thus the cutoff provided by the trap depth has a strong effect on the

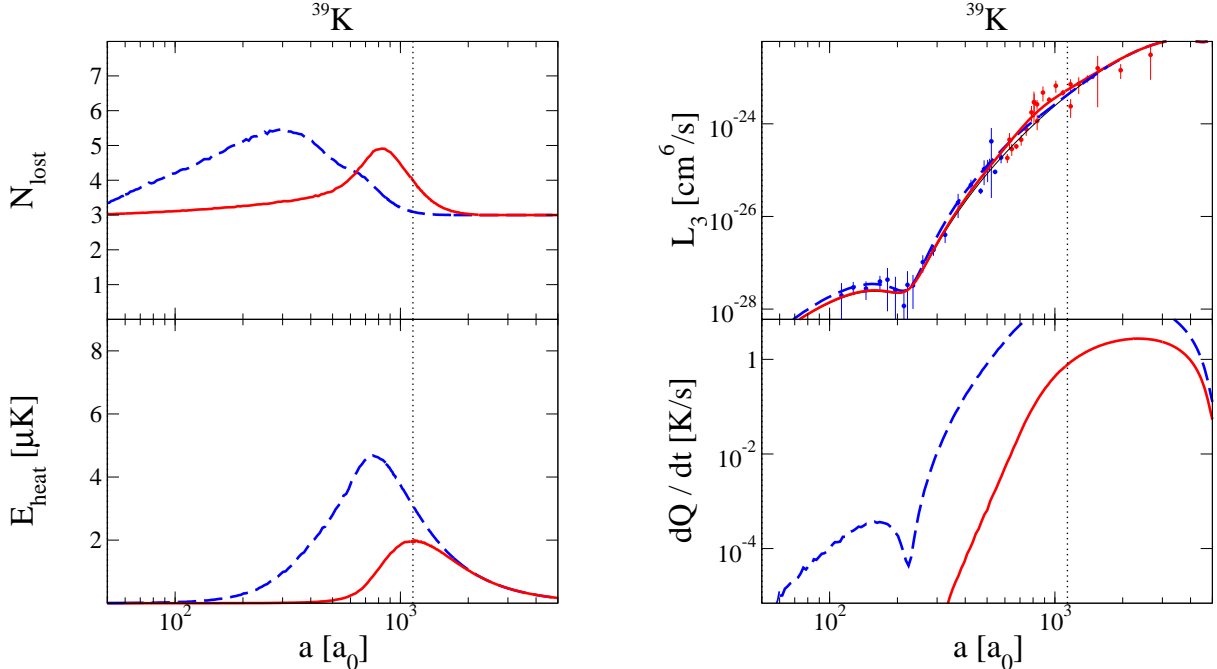


FIG. 3: (Color online) The average number N_{lost} of atoms lost in an avalanche (upper left panel), the average heat E_{heat} generated by an avalanche (lower left panel), the rate constant L_3 (upper right panel), and the heating rate dQ/dt (lower right panel) as functions of a . The system consists of ^{39}K atoms with $a_* = 1140 a_0$ and $\eta_* = 0.043$. The vertical dotted line marks the position of a_* . The universal prediction for L_3 without the avalanche mechanism is shown as a thin (black) line that provides a lower bound on the other curves. Over most of the range of a , it is covered up by one of the other curves. The dashed (blue) curves and the solid (red) curves are for the BEC and the thermal gas in Ref. [9], respectively. The data for L_3 are from the Florence group [9].

position of the peaks in N_{lost} and E_{heat} .

In the right panels of Fig. 3, the rate constant L_3 and the heating rate dQ/dt are shown as functions of a . The panel for L_3 in Fig. 3 shows the data from the Florence group [9]. The result for L_3 is visibly larger than the universal result without the avalanche mechanism in the region just below the local minimum near $e^{-\pi/s_0}a_+ = 225 a_0$ for the BEC and in the region just below $a_* = 1140 a_0$ for the thermal gas. Thus the avalanche mechanism can affect the fitted values of the Efimov parameters a_* and η_* . Both L_3 and dQ/dt have local minima near $e^{-\pi/s_0}a_+ = 225 a_0$ that arise from Efimov interference. The heating rate dQ/dt in the thermal gas is more than an order of magnitude smaller than in the BEC over most of the range of a .

B. ^7Li atoms

In 2009, the Rice group observed a peak in L_3/a^4 near $608 a_0$ in a BEC of ^7Li atoms in the $|1, +1\rangle$ hyperfine state [10]. This loss feature is near the predicted position of an atom-dimer resonance. Different experimental variables were used in different regions of the scattering length. The experimental variables used in one of these regions are listed in Table I. The Efimov parameters determined from the narrow loss minimum near $2676 a_0$ are $a_* = 598 a_0$

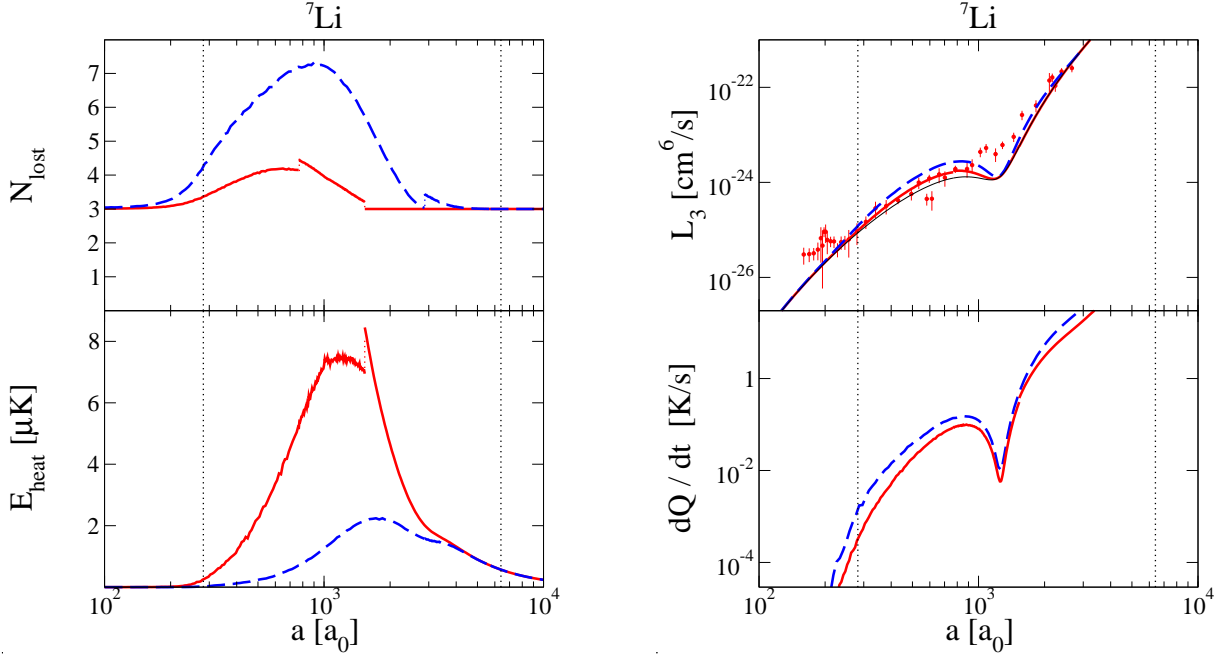


FIG. 4: (Color online) Same as Fig. 3, but for ${}^7\text{Li}$ atoms with $a_* = 282 a_0$ and $\eta_* = 0.039$. The dashed (blue) curves and the solid (red) curves are for the BEC in Ref. [10] and the thermal gas in Ref. [11], respectively. The data for L_3 are from the Bar-Ilan group [11].

and $\eta_+ = 0.039$. The Rice group has improved the accuracy of the determination of a as a function of the magnetic field and a reanalysis of the data from Ref. [10] is underway [16]. Their new analysis will not have a significant effect on the value of η_* , but it will shift the value of a_* closer to the value measured by the Bar-Ilan group, which is given below.

In 2010, the Bar-Ilan group observed a local minimum in L_3/a^4 in a thermal gas of ${}^7\text{Li}$ atoms in the $|1, +1\rangle$ hyperfine state [17]. The Efimov parameters determined by fitting their measurements of L_3 are $a_* = 282 a_0$ and $\eta_* = 0.188$. Since the van der Waals length for ${}^7\text{Li}$ atoms is $65 a_0$, the predicted atom-dimer resonance is safely in a universal region of large scattering length. In 2012, they presented additional data that revealed a narrow enhancement in L_3 near $200 a_0$, which is near the predicted atom-dimer resonance [11]. The experimental variables used in the measurement of L_3 are listed in Table I.

The Rice group and the Bar-Ilan group used the same hyperfine state of ${}^7\text{Li}$, so they should obtain the same Efimov parameters to within experimental errors. Since η_* is particularly sensitive to the width of the loss minimum at a_+ , thermal smearing and limited experimental resolution are most likely to lead to an overestimate of η_* . For the Efimov parameters, we will therefore use the value of a_* obtained by the Bar-Ilan group but the smaller value of η_* obtained by the Rice group: $a_* = 282 a_0$ and $\eta_* = 0.039$.

In the left panels of Fig. 4, the average number N_{lost} of atoms lost and the average heat E_{heat} from the avalanche are shown as functions of a for the two sets of experimental variables for ${}^7\text{Li}$ atoms listed in Table I. There are visible discontinuities in N_{lost} and E_{heat} at the scattering lengths at which $E_d = \frac{3}{2}E_{\text{trap}}$ and $E_d = 6E_{\text{trap}}$. These discontinuities are artifacts of our simple model for the trap depth. The number N_{lost} has a broad peak with a maximum value near 7 for the BEC and near 4 for the thermal gas. The position of the peak is at $905 a_0$ for the BEC and at $767 a_0$ for the thermal gas. This position is determined

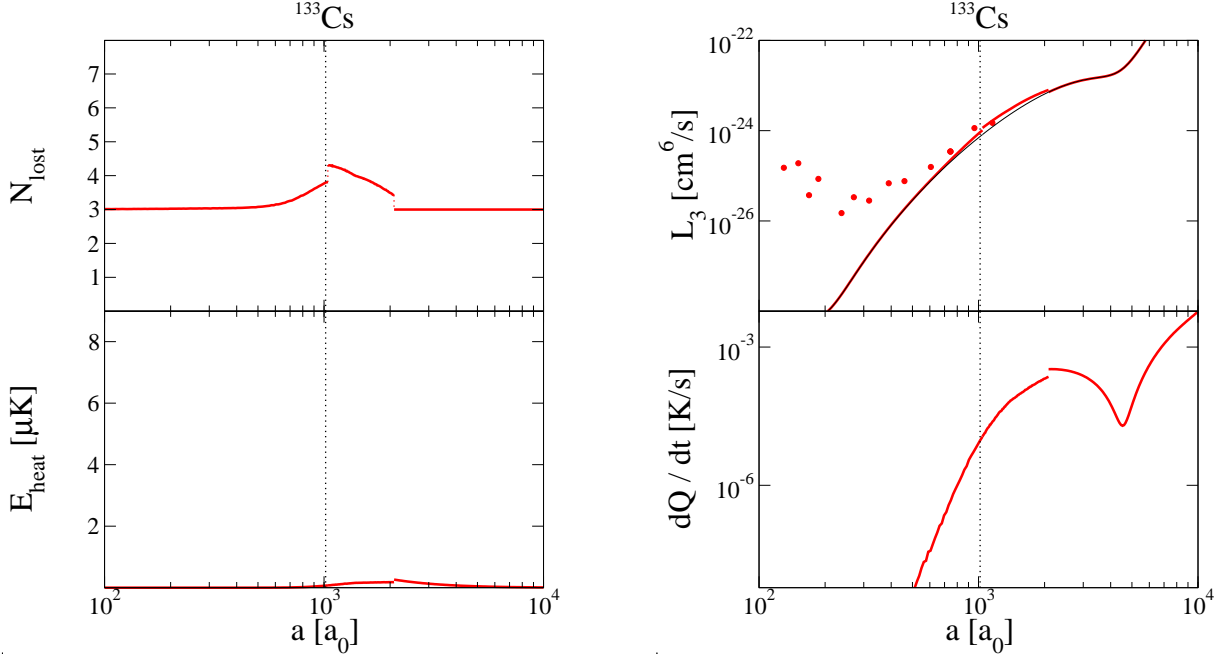


FIG. 5: (Color online) Same as Fig. 3, but for ^{133}Cs atoms with $a_* = 1017 a_0$ and $\eta_* = 0.08$. The solid (red) curves are for the thermal gas in Ref. [19]. The data for L_3 are from Ref. [19].

the scattering cross sections and the trap depth, among other things. The cross section for the first elastic scattering of the recombination dimer has a broad peak with its maximum at $4.34a_* \approx 1220 a_0$. The trap depth forces N_{lost} to decrease to the naive value 3 near $a = 5740 a_0$ for the BEC and near $a = 1530 a_0$ for the thermal gas. This cutoff provided by the trap depth has a strong effect on the position of the peaks in N_{lost} and E_{heat} .

In the right panels of Fig. 4, the rate constant L_3 and the heating rate dQ/dt are shown as functions of a . The panel for L_3 in Fig. 4 shows the data from the Bar-Ilan group [17]. The curves for L_3 have a much more pronounced local minimum at $a_+ \approx 1260 a_0$ than the data, because we have used the Efimov parameter $\eta_* = 0.039$ from the Rice experiment [10] instead of the value $\eta_* = 0.188$ obtained by fitting the Bar-Ilan data. For both the BEC and the thermal gas, the result for L_3 in the region just below the local minimum near $a_+ = 1260 a_0$ is visibly larger than the universal result without the avalanche mechanism. Since the Efimov parameters a_+ and η_* are sensitive to the position and width of the minimum, their fitted values can be strongly affected by the avalanche mechanism. Note that our Monte Carlo model predicts no peak in L_3 near the atom-dimer resonance at $a_* = 282 a_0$. Both L_3 and dQ/dt have local minima near $a_+ = 1260 a_0$ that arise from Efimov interference. The heating rates dQ/dt are similar in the BEC and in the thermal gas.

C. ^{133}Cs atoms

The Innsbruck group has studied loss features in thermal gases of ^{133}Cs atoms in several universal regions of the magnetic field. In 2005, they studied a region of low magnetic field and observed a local minimum of L_3/a^4 that can be attributed to Efimov interference at a scattering length near $210 a_0$ [6]. Setting $a_+ = 210 a_0$, atom-dimer resonances are predicted at $47 a_0$ and $1070 a_0$. Since the van der Waals length for ^{133}Cs atoms is $200 a_0$,

only the higher atom-dimer resonance is in a universal region of large scattering length. The Innsbruck group did not observe any loss feature near $1070 a_0$.

In 2011, the Innsbruck group observed three peaks in L_3/a^4 in different universal regions with large negative a at higher magnetic field [19]. They can all be attributed to resonant enhancement from an Efimov trimer near the 3-atom threshold. Two of these loss features are complicated by the presence of a G-wave Feshbach resonance. The Efimov parameters associated with the third loss feature are $a_- = -955 a_0$ and $\eta_* = 0.08$. The Innsbruck group found that the Efimov parameter a_- has almost the same value in all the universal regions, which suggests that it is determined by the van der Waals length [19]. The universal ratios in Eqs. (1) and (2) can be used to predict an atom-dimer resonance at $a_* = 1017 a_0$ and an Efimov interference minimum in L_3/a^4 near $a_+ = 200 a_0$. The Innsbruck group measured L_3 in a universal region of large positive a . They observed a local minimum near $270 a_0$, which is near the predicted position of a_+ , but they did not see any loss feature near a_* . The experimental variables used in this region of positive scattering length are listed in Table I.

In the left panels of Fig. 5, the average number N_{lost} of atoms lost and the average heat E_{heat} from the avalanche are shown as functions of a for this set of experimental variables. The number of lost atoms coincidentally has a peak very close to the atom-dimer resonance a_* but the peak in E_{heat} is at a higher value of a . The average heat E_{heat} is more than an order of magnitude smaller than in the ^7Li and ^{39}K thermal gas experiments described above.

In the right panels of Fig. 5, the rate constant L_3 and the heating rate dQ/dt are shown as functions of a . The increase in L_3 from the avalanche mechanism is visible only in the region just above $a_* = 1017 a_0$. Both L_3 and dQ/dt have local minima from Efimov interference near $a_+ = 4550 a_0$. The panel for L_3 in Fig. 5 also shows the data from the Innsbruck group [19]. There is a local minimum near $200 a_0$, which is near the predicted value of a_+ . The deviations between the measurements and the universal predictions at smaller a is not unexpected, because this is a nonuniversal region.

VI. DIMER-DIMER RESONANCES

We have used our Monte Carlo model for the avalanche mechanism to show that it cannot produce a narrow loss feature near an atom-dimer resonance. The essential reason is explained by the energy dependence of the elastic atom-dimer cross section, which is illustrated in Fig. 2. Since the shallow dimer from 3-body recombination loses energy with each elastic collision, the first few collisions of the dimer are those that are the most likely to knock an extra atom out of the trap. In the first few collisions, the dimer's kinetic energy is comparable to its binding energy E_d , and there is no dramatic enhancement of the atom-dimer cross section. Rather, the atom-dimer cross section is dramatically enhanced only after many elastic collisions have reduced the dimer's kinetic energy to much smaller than E_d . However, with its kinetic energy degraded, the dimer is much less likely to knock an atom out of the trap.

The universality of atoms with large scattering length is not limited to the 2-atom and 3-atom sectors. In 2004, Hammer, Meissner, and Platter made the first suggestion that universality should extend to the 4-atom sector [23]. They presented numerical evidence that there are two universal tetramers associated with each Efimov trimer, and they made the first calculations of the tetramer binding energies for some regions of $1/a$ [23, 24]. In 2008, von Stecher, D'Incao, and Greene calculated the tetramer binding energies more accurately

and over the entire range of $1/a$ [25]. They pointed out that the most dramatic signature of a universal tetramer is the resonant enhancement of the 4-body recombination rate at a negative value of a where the tetramer is at the 4-atom threshold. The loss features from a pair of universal tetramers were first observed by the Innsbruck group using a thermal gas of ^{133}Cs atoms [26]. They measured the 4-body loss rate constant L_4 for one of the tetramers. Universal tetramers have also been observed in a thermal gas experiment with ^7Li atoms by the Rice group [10]. They measured L_4 for both members of one pair of tetramers and for one member of another pair.

A universal tetramer could also produce loss features at positive values of a . One possibility is a loss feature at a scattering length at which a tetramer crosses the 2-dimer threshold, which we will refer to as a *dimer-dimer resonance*. The dimer-dimer elastic and inelastic cross sections are resonantly enhanced near threshold at a dimer-dimer resonance. Each Efimov trimer, with atom-dimer resonance at a_* , has associated with it two universal tetramers, with dimer-dimer resonances at larger scattering lengths a_{*1} and a_{*2} . The universal predictions for the positions of these dimer-dimer resonances were first calculated by von Stecher, D’Incao, and Greene [25]. They were recently calculated by Deltuva with 4 digits of precision [27]:

$$a_{*1} = 2.196 a_*. \quad (34a)$$

$$a_{*2} = 6.785 a_*. \quad (34b)$$

In their experiment with a BEC of ^7Li atoms, the Rice group observed narrow enhancements in the measured 3-body loss rate constant L_3 near $+1470 a_0$ and near $+3910 a_0$ [10]. These scattering lengths are near the predicted positions of the two dimer-dimer resonances for a pair of universal tetramers. These loss features are even more mysterious than those near atom-dimer resonances. Three-body recombination can create a shallow dimer with kinetic energy comparable to E_d . Four-body recombination can create one or two shallow dimers with kinetic energy comparable to E_d . If the equilibrium population of shallow dimers in the atom cloud is negligible, the recombination dimers can only undergo atom-dimer collisions. Thus the resonant enhancement of dimer-dimer cross sections near a dimer-dimer resonance should have no effect on the atom loss rate. Therefore, there is no analog of the avalanche mechanism near a dimer-dimer resonance.

One possible explanation for the narrow loss features near the atom-dimer and dimer-dimer resonances is that the equilibrium population of shallow dimers in the atom cloud is not negligible. The resonant enhancement of the inelastic atom-dimer cross section could then produce an enhanced loss rate near a_* . Similarly, the resonant enhancement of the inelastic dimer-dimer cross section could produce enhanced loss rates near a_{*1} and near a_{*2} . The number density n_d of the dimers must be much smaller than the number density n of the atoms. In the absence of atom loss processes, the rates of atom-dimer and dimer-dimer collisions would be proportional to nn_d and n_d^2 , respectively. If n_d is proportional to n^2 , the atom-dimer and dimer-dimer collision rates have the same dependence on n as the 3-body and 4-body recombination rates, respectively. Thus the enhanced loss rate near a_* from low-energy inelastic atom-dimer collisions would manifest itself as an apparent enhancement of the 3-body recombination rate. Similarly, enhanced loss rates near a_{*1} and near a_{*2} from low-energy inelastic atom-dimer collisions would manifest themselves as apparent enhancements in the 4-body recombination rate. While an equilibrium population of dimers could explain the existence of loss features at the atom-dimer and dimer-dimer resonances, it can not easily account for them quantitatively. It seems likely that a population of dimers large enough to

account for the observed loss features should also have been observed more directly.

Narrow loss features have been observed near atom-dimer resonances in several experiments and near dimer-dimer resonances in the ^7Li BEC experiment. We have shown that the avalanche mechanism cannot produce a narrow loss feature near an atom-dimer resonance. It also cannot produce any loss of atoms near a dimer-dimer resonance. An equilibrium population of dimers could produce loss features near atom-dimer and dimer-dimer resonances, but a population of dimers large enough to account for the observed loss features should probably have been observed more directly. We suggest that another mechanism that has not yet been identified must be responsible for the loss features that have been observed near atom-dimer and dimer-dimer resonances.

Acknowledgments

We thank R. Grimm, R. Hulet, L. Khaykovich, H.-C. Nägerl, and M. Zaccanti for useful communications. We also thank M. Zaccanti, L. Khaykovich, and M. Berninger and A. Zenesini for providing their data. This research was supported in part by a joint grant from the Army Research Office and the Air Force Office of Scientific Research.

-
- [1] E. Braaten and H.-W. Hammer, “Universality in Few-body Systems with Large Scattering Length,” *Phys. Rept.* **428**, 259 (2006).
 - [2] V. Efimov, “Energy Levels Arising from Resonant Two-body Forces in a Three-body System,” *Phys. Lett.* **33B**, 563 (1970).
 - [3] V. Efimov, “Energy Levels of Three Resonantly-interacting Particles,” *Nucl. Phys. A* **210**, 157 (1973).
 - [4] V. Efimov, “Low-energy Properties of Three Resonantly-interacting Particles,” *Sov. J. Nucl. Phys.* **29**, 546 (1979) [*Yad. Fiz.* **29**, 1058 (1979)].
 - [5] B.D. Esry, C.H. Greene, and J.P. Burke, “Recombination of Three Atoms in the Ultracold Limit,” *Phys. Rev. Lett.* **83**, 1751 (1999).
 - [6] T. Kraemer et al., “Evidence for Efimov Quantum States in an Ultracold Gas of Caesium Atoms,” *Nature* **440**, 315 (2006). [arXiv:cond-mat/0512394].
 - [7] E. Braaten and H.-W. Hammer, “Enhanced Dimer Deactivation in an Atomic/Molecular BEC,” *Phys. Rev. A* **70**, 042706 (2004).
 - [8] S. Knoop et al., “Observation of an Efimov-like resonance in ultracold atom-dimer scattering,” *Nature Physics* **5**, 227 (2009). [arXiv:0807.3306].
 - [9] M. Zaccanti et al., “Observation of an Efimov spectrum in an atomic system,” *Nature Physics* **5**, 586 (2009) [arXiv:0904.4453].
 - [10] S.E. Pollack, D. Dries, and R.G. Hulet “Universality in Three- and Four-Body Bound States of Ultracold Atoms,” *Science* **326**, 1683 (2009) [arXiv:0911.0893].
 - [11] O. Machtey et al., “Association of Efimov trimers from three-atoms continuum,” *Phys. Rev. Lett.* **108**, 210406 (2012) [arXiv:1201.2396].
 - [12] C. Langmack, D.H. Smith, and E. Braaten “The Avalanche Mechanism for Atom Loss near an Atom-Dimer Efimov Resonance,” *Phys. Rev. A* **86**, 022718 (2012) [arXiv:1205.2683].
 - [13] A. Deltuva, “Properties of universal bosonic tetramers,” [arXiv:1202.0167].

- [14] K. Helfrich, H.-W. Hammer, and D.S. Petrov, “Three-body problem in heteronuclear mixtures with resonant interspecies interaction,” *Phys. Rev.* **A81**, 042715 (2010) [arXiv:1001.4371].
- [15] C. Ji, D. R. Phillips and L. Platter, “The three-boson system at next-to-leading order in an effective field theory for systems with a large scattering length,” *Ann. Phys.* **327**, 1803 (2012).
- [16] R.G. Hulet, private communication.
- [17] N. Gross, Z. Shotan, S. Kokkelmans, and L. Khaykovich, “Nuclear-Spin-Independent Short-Range Three-Body Physics in Ultracold Atoms,” *Phys. Rev. Lett.* **105**, 103203 (2010) [arXiv:1003.4891].
- [18] N. Gross, Z. Shotan, O. Machtey, S. Kokkelmans, and L. Khaykovich, “Study of Efimov physics in two nuclear-spin sublevels of ^7Li ,” *C. R. Physique* **12**, 4 (2011) [arXiv:1009.0926].
- [19] M. Berninger et al., “Universality of the Three-Body Parameter for Efimov States in Ultracold Cesium,” *Phys. Rev. Lett.* **107**, 120401 (2011) [arXiv:1106.3933].
- [20] O. Machtey, D.A. Kessler, and L. Khaykovich, “Universal Dimer in a Collisionally Opaque Medium: Experimental Observables and Efimov Resonances,” *Phys. Rev. Lett.* **108**, 130403 (2012) [arXiv:1111.5503].
- [21] E. Braaten, H. -W. Hammer, D. Kang and L. Platter, “Three-Body Recombination of Identical Bosons with a Large Positive Scattering Length at Nonzero Temperature,” *Phys. Rev. A* **78**, 043605 (2008) [arXiv:0801.1732].
- [22] T. Weber et al., “Three-Body Recombination at Large Scattering Lengths in an Ultracold Atomic Gas,” *Phys. Rev. Lett.* **91**, 123201 (2003) [arXiv:physics/0304052].
- [23] L. Platter, H. W. Hammer and U. -G. Meissner, “The Four boson system with short range interactions,” *Phys. Rev. A* **70**, 052101 (2004) [cond-mat/0404313].
- [24] H. -W. Hammer and L. Platter, *Eur. Phys. J. A* **32**, 113 (2007) [nucl-th/0610105].
- [25] J. von Stecher, J.P. D’Incao, and C.H. Greene, “Four-body legacy of the Efimov effect,” *Nature Physics* **5**, 417 (2009) [arXiv:0810.3876].
- [26] F. Ferlaino et al., “Evidence for Universal Four-Body States Tied to an Efimov Trimer,” *Phys. Rev. Lett.* **102**, 140401 (2009) [arXiv:0903.1276].
- [27] A. Deltuva, “Universality in bosonic dimer-dimer scattering,” *Phys. Rev. A* **84**, 022703 (2011) [arXiv:1107.3956].